

Hybrid Si-GaAs photonic crystal cavity for lasing and bistability

Mohammad Habibur Rahaman^{1,2}, Chang-Min Lee^{1,2}, Mustafa Atabey Buyukkaya^{1,2}, Yuqi Zhao^{1,2}, Edo Waks^{1,2,3,4}

¹Department of Electrical and Computer Engineering, University of Maryland, College Park, Maryland, USA, 20742.

²Institute for Research in Electronics and Applied Physics (IREAP), University of Maryland, College Park, Maryland, USA, 20742.

³Department of Physics, University of Maryland College Park, MD, 20742.

⁴Joint Quantum Institute (JQI), University of Maryland, College Park, MD, 20742.

Corresponding author, edowaks@umd.edu

Abstract. The heterogeneous integration of silicon with III-V materials provides a way to overcome silicon's limited optical properties toward a broad range of photonic applications. Hybrid modes are a promising way to make heterogeneous Si/III-V devices, but it is still unclear how to engineer these modes to make photonic crystal cavities. Herein, using 3D finite-difference time-domain simulation, a hybrid Si-GaAs photonic crystal cavity design enables cavity mode confinement in GaAs without directly patterning that operates at telecom wavelengths. The hybrid cavity consists of a patterned silicon waveguide nanobeam that is evanescently coupled to a GaAs slab with quantum dots. We show that by engineering the hybrid modes, we can control the degree of coupling to the active material, which leads to a tradeoff between cavity quality factor and optical gain and nonlinearity. With this design, we demonstrate a cavity mode in the Si-GaAs heterogeneous region, which enables strong interaction with the quantum dots in the GaAs slab for applications such as low-power-threshold lasing and optical bistability (156 nW and 18.1 μ W, respectively). This heterogeneous integration of an active III-V material with silicon via a hybrid cavity design suggests a promising approach for achieving on-chip light generation and low-power nonlinear platforms.

1. Introduction

Silicon is a promising candidate for photonic integrated circuits due to its low power consumption, low cost, and high integration density.¹ Additionally, silicon on an insulator provides a high index contrast platform^{2,3} that enables the fabrication of extremely compact passive optical devices, such as low loss waveguides^{4,5}, grating couplers^{6,7}, mode converters⁸, multiplexers⁹, and more. However, silicon lacks active optical properties due to its indirect bandgap, which has impeded the development of silicon-based photonic integrated circuits. As an alternative, direct bandgap III-V semiconductors (e.g., GaAs) offer significant active optical properties such as light emission and absorption at telecom wavelengths. In particular, III-V nanophotonic devices can implement low threshold lasers^{10,11}, amplifiers¹¹, modulators,¹² and highly nonlinear devices¹³. The integration of III-V nanophotonic devices with silicon could pave the way towards ultra-compact low energy nanophotonic and opto-electronic devices. Researchers have increasingly explored the heterogeneous integration of III-V materials with silicon to utilize the advantages of both systems^{2,14}.

There has been significant progress in hybrid integration of silicon and III-V nanophotonics. Nanophotonic heterogeneous integration has also been achieved in several nanolaser designs.^{15–19} In all of these cases, hybrid integration was achieved by placing a III-V nanophotonic device in close proximity to a silicon waveguide and relying on evanescent coupling between the two structures. This approach

requires careful placement and alignment of the nanophotonic cavity in the evanescent field of the waveguide in order to achieve efficient coupling. But such active alignment can significantly complicate the design and fabrication of integrated photonic devices.²⁰ Hybrid photonic modes offer an alternate approach to couple silicon and III-V semiconductors. In this approach, the mode of a silicon waveguide is carefully engineered to hybridize with a III-V semiconductor layer that serves as the active material.²¹ Hybrid modes have been used to engineer laser sources,^{21,22} amplifiers,²³ and modulators.²⁴ But all of these works exploit hybrid modes of a silicon waveguide. The use of hybrid modes to engineer nanophotonic devices remains far less explored.

In this letter we propose and analyze a hybrid mode approach to engineer Si-GaAs nanophotonic cavity without the need for careful active alignment that enables low power threshold lasing and optical bistability. Unlike previous hybrid integration approaches where a silicon waveguide is coupled to a GaAs nanophotonic device, the hybrid mode cavity utilizes a patterned silicon cavity structure coupled to a planar GaAs slab that contains the active material. This approach alleviates the need for careful alignment between a silicon photonic waveguide and III-V semiconductor device. We numerically design and characterize the structure using 3D finite-difference time-domain (FDTD) method coupled to a Maxwell-Bloch equation model that accounts for the active material in the GaAs slab.^{25,26} We show that the hybrid cavity mode can exhibit a low lasing threshold of just 156 nW, which we attribute to the high spontaneous emission coupling ratio enabled by the low mode volume of the active media in the hybrid cavity.²⁷ Additionally, under continuous wave operation, we found a low optical bistability threshold of 18.1 μ W. This hybrid Si-GaAs cavity design can also be optimized for different operating frequencies and integration with other active materials beyond quantum dots, such as Kerr nonlinear media.²⁸ This approach could enable simpler more scalable approach to heterogeneous integration of III-V materials with silicon nanophotonics.

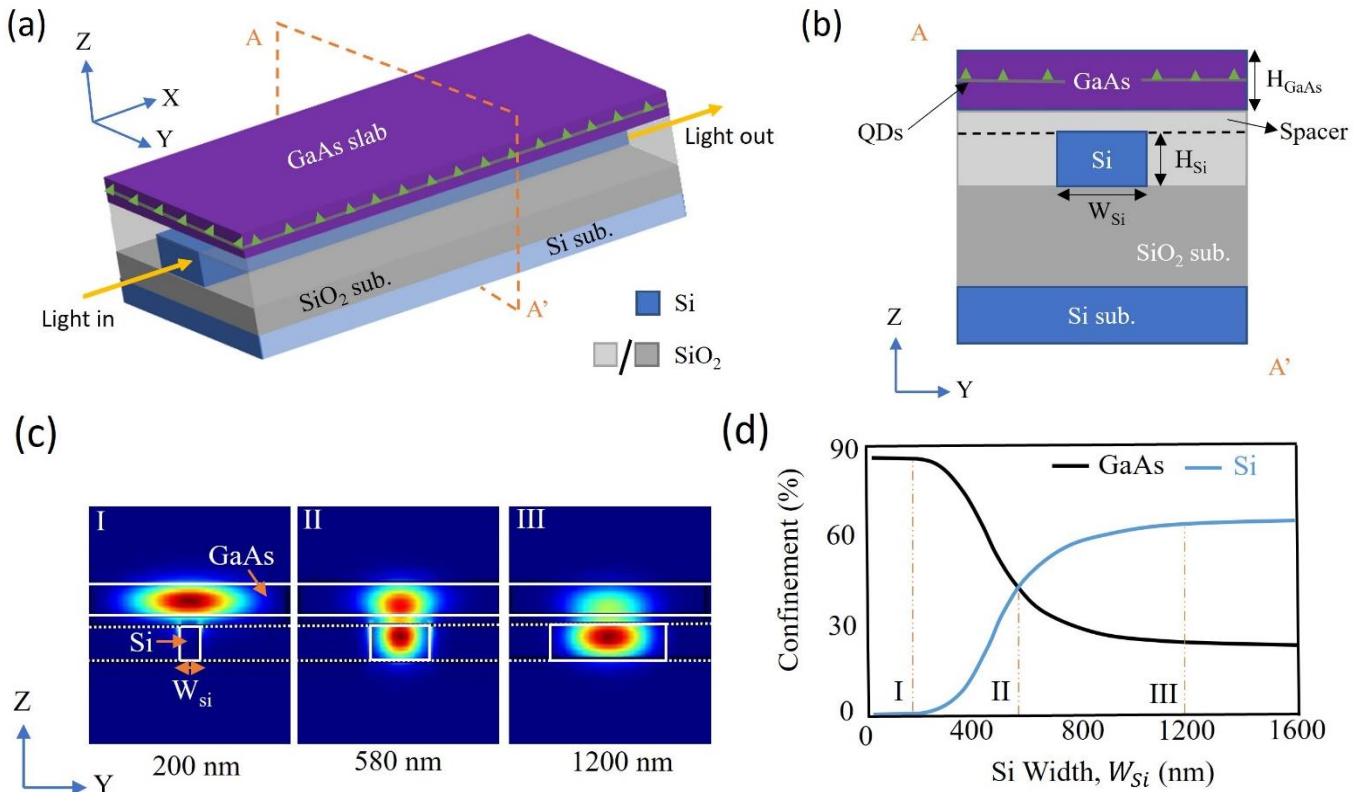


Figure 1. (a) 3D Schematic illustration of the Si-GaAs hybrid cavity, and (b) the corresponding 2D cross-section. (c) The transverse mode profile ($|E|$) of the hybrid mode for different silicon waveguide widths (W_{Si}) of 200 nm, 580 nm, and 1200 nm at a fixed GaAs slab width of 2 μm at an incident light wavelength of 1516.53 nm. The white lines represent the boundaries of the silicon waveguide and GaAs slab. (d) The silicon waveguide width controls the relative confinement of the hybrid mode in the silicon waveguide and GaAs slab region, where positions I, II, and III correspond to different silicon waveguide widths marked in (c).

2. Proposed hybrid Si-GaAs cavity design

We first analyze the hybrid mode structure of a silicon waveguide coupled to a GaAs slab. Figure 1a, b illustrates the hybrid structure which is composed of a silicon waveguide with height H_{Si} and width W_{Si} . The waveguide is embedded in an SiO_2 cladding layer. A GaAs slab of thickness H_{GaAs} and width W_{GaAs} embedded with active material (e.g., quantum wells or quantum dots) is placed on top of the silicon waveguide separated by a spacer with thickness t .

We simulate the mode structure of the waveguide by direct eigenmode expansion (ANSYS MODE solutions). We consider the case where $t = 60 \text{ nm}$, $H_{Si} = 220 \text{ nm}$, $H_{GaAs} = 200 \text{ nm}$ and $W_{GaAs} = 2 \mu\text{m}$. Figure 1c shows the transverse mode profile of the waveguide modes for several different values of w . Consistent with previous work on hybrid modes², as the width of the waveguide increases from 200 nm to 1200 nm the guided mode continuously shifts from being predominantly confined in the GaAs slab to being confined in the silicon waveguide. Figure 1d shows confinement factor in silicon and GaAs region, defined as $\int_{Si \text{ or } GaAs} |E|^2 dA / \int_{total} |E|^2 dA$, which shows the gradual shift between the two materials. The three vertical dashed lines labeled I, II, and III correspond to the widths plotted in Fig. 1c.

Without the GaAs layer, this device structure would lead to a highly localized cavity mode within the silicon waveguide. But adding the GaAs layer causes the mode to hybridize. The key to designing the cavity mode is to carefully select the width W_{Si} . If this width is made to be large, most of the mode will be confined in silicon leading to strong optical confinement but poor overlap with the GaAs active material. In contrast, if W_{Si} is made too small the majority of the hybrid mode will be confined to the GaAs active material where it can experience large gain and nonlinearity. But in this regime the effective index contrast of the photonic crystal will be low which will result in poor optical confinement and low quality factors. The width must therefore be carefully designed to balance out these conflicting requirements.

To design the cavity, we first analyze a periodic photonic crystal waveguide. We choose ellipsoidal cavity with a lattice period a of 380 nm and radii of 140 nm and 130 nm for the major and minor axes of the elliptical cavities, respectively. We select the width of the waveguide to be 580 nm, which creates hybrid mode that is nearly equally confined in both the silicon and GaAs (see Figure 1c). This value provides a good compromise between mode confinement and overlap with the active material. We calculate the photonic band structure by performing three-dimensional Finite Difference Time Domain simulations (ANSYS FDTD solution) with Bloch boundary conditions. Figure 2a shows the optimized photonic band-structure, which features a sufficiently wide photonic bandgap of 8.5 THz that spans within a telecom range of 192 THz to 200.5 THz (grey shaded region).

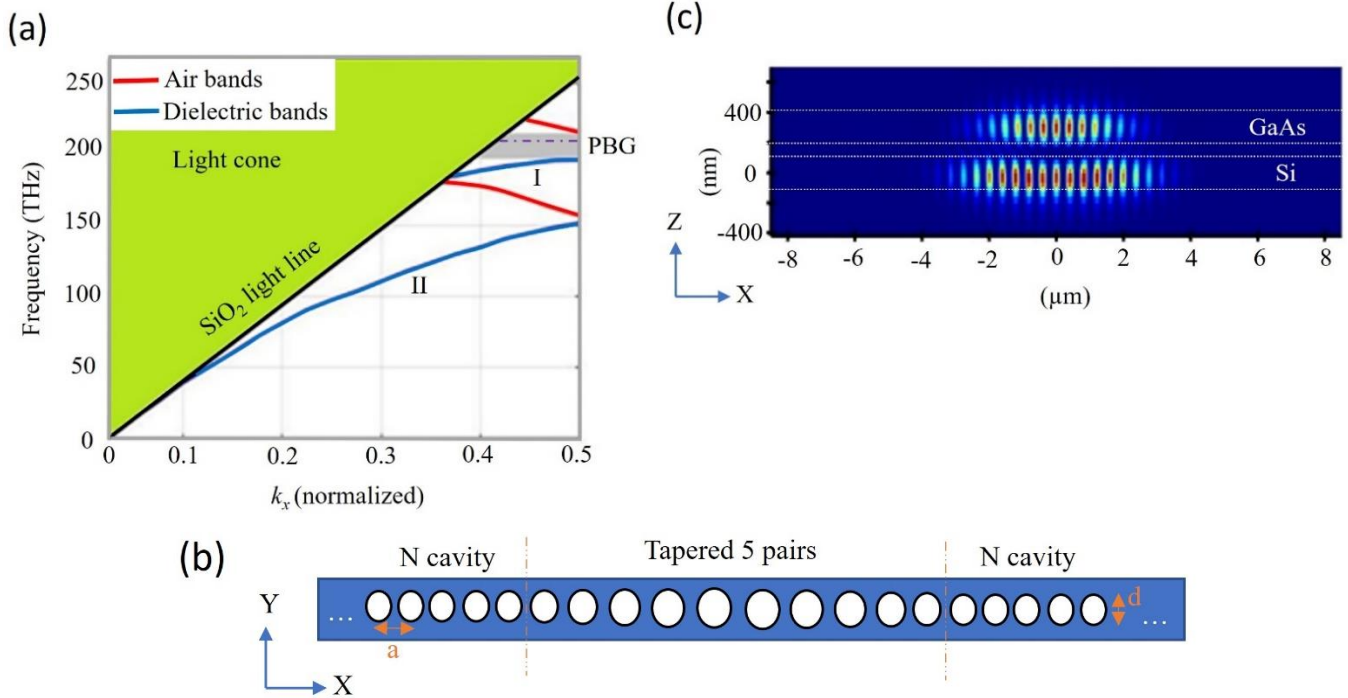


Figure 2. (a) The FDTD calculated band structure of the hybrid Si-GaAs device. The grey shaded area is the photonic bandgap (PBG), which corresponds to the difference between the calculated air bands (red curves) and dielectric bands of the silicon and GaAs (blue curves marked I and II, respectively). Here, k_x is related to wavevector $k = k_x (2\pi/a)$, which is a function of the reciprocal lattice parameter a specified by the Bloch boundary condition. The black line denotes the SiO₂ light line, and the horizontal purple dashed line in PBG indicates the cavity resonance frequency. (b) Schematic diagram of the silicon waveguide cavity design, which features a total of 16 cavity pairs, including $N = 11$ ellipsoidal cavities on both sides and 5 centered pairs of tapered ellipsoids as defects. (c) The fundamental mode field ($|E|$) profile in the hybrid Si-GaAs cavity obtained using the 3D FDTD method. The white dashed lines denote the silicon and GaAs layers (220 nm and 200 nm thick, respectively), which are separated by a 60 nm spacer.

In order to create a cavity mode, we introduce a defect into the photonic crystal waveguide. The defect is composed of a taper where we linearly increase both the major and minor axes of the elliptical holes. Figure 2b shows the structure of the defect corresponding to five center pairs of holes taper where we increase the major axes of the ellipses from 140 nm to 150 nm, and the minor axes increase from 130 nm to 140 nm. Figure 2c plots the electric field profile $|E|$ at resonance wavelength 1516.53 nm of this hybrid Si-GaAs cavity, which reveals a fundamental cavity mode that extends in both the silicon waveguide and GaAs slab (Figure 2c). The mode is highly localized in the cavity region and has a substantial overlap with both the silicon and GaAs region. It thus achieves a hybrid localized photonic crystal cavity mode. We calculate the mode volume to be $V_m \sim 2 (\lambda/n)^3$, and the quality factor to be $Q = 1.53 \times 10^4$.

3. Lasing

The hybrid mode cavity has the potential to achieve tight optical confinement with high-quality factors, making it a promising candidate for low-threshold lasers. These lasers exploit enhanced spontaneous emission into the lasing mode, which leads to a high spontaneous emission coupling ratio.²⁹ To numerically simulate lasing from the hybrid cavity, we focus on the specific case where the active material

in the GaAs layer is composed of InAs quantum dots. The quantum dots can be described by a four-level atom model.^{25,26} In our numerical simulation, we employ a pump of 750 nm wavelength with a pulse width of 4.5 ps and a broadband probe of two orders of magnitude smaller than the pump amplitude centered at the hybrid cavity resonance wavelength of 1516.53 nm. In the four-level model, we use an initial population volume density of $N_1 = N_0 = 7 \times 10^{21}/\text{m}^3$.

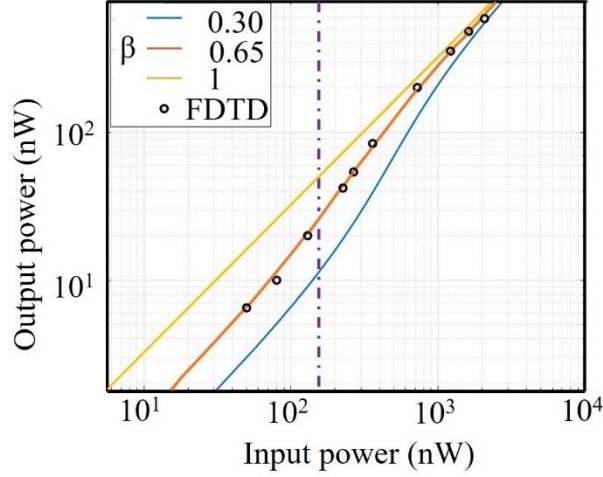


Figure 3. Using 3D FDTD, we calculate the input power versus output power (log-log L-L curve) of the hybrid Si-GaAs cavity nanolaser (black circles) and fit the results using a rate equation model (Equation 1) as shown by the orange curve, which correspond to spontaneous emission coupling ratios of $\beta = 0.65$. The yellow and blue solid curves are also plotted using rate equation with spontaneous emission coupling ratios of $\beta = 0.3$ and 1 , respectively. The vertical dashed line is the lasing threshold obtained from the rate equation fit to the FDTD data.

To investigate the lasing capabilities of the hybrid Si-GaAs cavity, we use 3D FDTD to calculate the cavity output power as a function of the input pump power (L-L curve) using the pump-probe technique. Light enters and is coupled in-plane within the heterogeneous region of the silicon and GaAs with the resulting light transmitting from the other side of the device (Figure 1a). Figure 3 plots the FDTD calculations (black circles), which is fitted by the solid lines using the cavity laser rate-equation model given by³⁰

$$P_{in} = \frac{\hbar\omega\gamma}{\beta\eta_{in}} \left[\frac{p}{1+p} (1 + \zeta)(1 + \beta p) - \zeta\beta p \right] \quad (1)$$

Here, P_{in} is the input pump power, ω is the cavity resonance frequency, $\gamma = \omega/Q$ is the cavity decay rate, and β is the spontaneous emission coupling ratio. We define the cavity photon number as $p = P_{out}/\hbar\omega\gamma\eta_{out}$, where η_{out} is the output collection efficiency of the laser. Additionally, η_{in} is the pumping efficiency, and ζ is the cavity photon number at transparency.

From Equation 1, we calculate several L-L curves corresponding to spontaneous emission coupling ratios and find the FDTD lasing data is best fit by a spontaneous emission coupling ratio of 0.65 (orange curve). We then calculate the lasing threshold power from the condition when there is an average of one photon in the cavity ($p = 1$). Using this value of p in Equation 1, we obtain a threshold power of $P_{th} = 156$ nW

which is shown by the vertical dashed line. We also plot L-L curves corresponding to spontaneous emission coupling ratios of $\beta = 0.3$ (blue curve) and 1 (yellow curve) for reference. A laser with large β decreases the lasing threshold, and for $\beta=1$, the laser has no threshold, while decreasing β increases the lasing threshold (e.g., $\beta=0.3$). A hallmark feature of lasing is an increase in the slope of the log-log curve near the lasing threshold,^{31,32} as we observe in the FDTD data (black circles). Our simulation demonstrates a lower lasing threshold compared to other devices using hybrid Si-III/V materials,^{15–19} which have previously reported a lasing threshold power as low as $1 \mu\text{W}$.¹⁹

4. Bistability

Optical bistability, a nonlinear optical phenomenon, can be defined as an optical system possessing two different output states corresponding to the same input intensity. The optical bistability of two-level atoms confined in an optical cavity is particularly useful for a wide range of applications, including all-optical switches,³³ memories,³⁴ optical logic gates,³⁵ and optical transistors.³⁶ Our hybrid cavity can operate as a low-power bistable device by employing such optical nonlinearity. Specifically, we use a two-level one electron numerical model to simulate the quantum dots as saturable absorbers in the hybrid Si-GaAs cavity.^{37,38} Here we use two-level quantum dots for bistability analysis instead of four-level quantum dots used for lasing calculation in the previous section because it is faster to simulate, and this analysis does not require gain media. To simulate the optical response of the InAs quantum dots in the GaAs region of the hybrid cavity, we incorporate the Maxwell-Bloch equations into numerical FDTD simulations using the method described by Shih-Hui Chang and Allen Taflove.²⁵ The Maxwell Bloch equations describe the response of saturable absorbers to an incident electric field.

$$\frac{dN_{11}}{dt} = -i\frac{\Omega}{2}(\chi_{SA}^* - \chi_{SA}) + \gamma N_{22} \quad (2)$$

$$\frac{dN_{22}}{dt} = i\frac{\Omega}{2}(\chi_{SA}^* - \chi_{SA}) - \gamma N_{22} \quad (3)$$

$$\frac{d\chi_{SA}}{dt} = -(\beta + i\Delta)\chi_{SA} - i\frac{\Omega}{2}(N_{22} - N_{11}) \quad (4)$$

Here, N_{11} and N_{22} are the population densities of the two-level atoms for the ground and excited states, $\Omega = \mu E/\hbar$ is the optical Rabi frequency, and μ is the transition matrix elements of the two-level atom. We define the detuning frequency as $\Delta = \omega_0 - \omega$, while ω_0 and ω are the resonant frequency and incident light frequency. We also describe the atomic decay rate as $\gamma = \gamma_{non} + \gamma_{rad}$, where γ_{non} is the nonradiative decay rate and $\gamma_{rad} = \frac{\mu^2 \omega^3}{3\pi\hbar\epsilon_0(1+\chi_D)c^3}$ is the radiative decay rate. Finally, $\beta = \gamma/2 + 1/T_2$, while T_2 is the dipole dephasing time.

For the simulation parameters, we set a layer of InAs quantum dots in the GaAs region of the hybrid cavity at a planar quantum dot density of $N = 7 \times 10^{10} / \text{cm}^2$.³⁹ We set the decay rates of the quantum dots to their room temperature values of $\gamma_{rad} = 1 \text{ GHz}$ ⁴⁰ and $\gamma_{non} = 1 \text{ GHz}$,⁴¹ and the dephasing time to $T_2 = 300 \text{ fs}$.⁴²

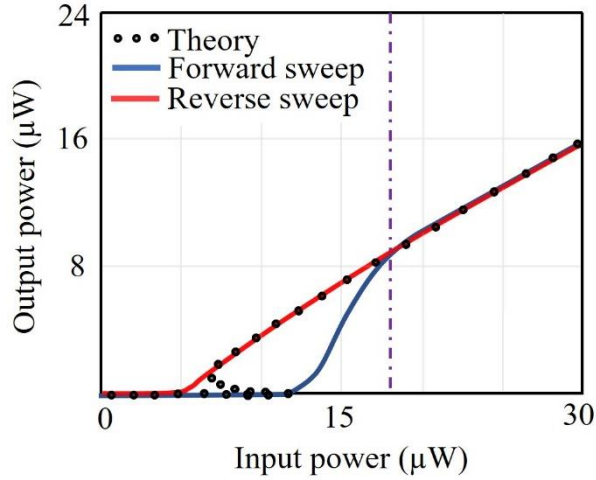


Figure 4. Output power vs. input power at the resonance wavelength 1516.53 nm of the hybrid Si-GaAs cavity, featuring quantum dots as saturable absorbers in the GaAs slab. The blue and red curves are the forward and reverse sweeps of the input intensity, while the black circles represent the theoretical bistability curve. The vertical purple dashed line is the bistability threshold.

Figure 4 plots the on-resonance bistability in the hybrid cavity for in-plane (Figure 1a) continuous wave excitation at 1516.53 nm. Theoretically, the output intensity is a bistable function of the cavity input at a steady state, as shown by the green dashed line in Figure 4 corresponds to the following equation^{43,44}

$$y = x + \frac{2Cx}{1+x^2} \quad (5)$$

Where $C = \alpha L/2T$ is the co-operativity parameter, with α being the absorption coefficient, and x and y are the output field amplitude and input field amplitude. We evaluate the co-operativity parameter $C = 10.49$ from FDTD calculated atomic-absorption coefficient $\alpha = 1.37 \times 10^4 \text{ cm}^{-1}$.

However, in FDTD, we observe a hysteretic behavior in the output intensity depending on whether the input intensity is increasing or decreasing (blue and red curves, respectively).⁴⁵ Bistable loop of output power provides the bistability threshold power, which occurs at 18.1 μW according to our FDTD calculations (vertical purple dashed line). The low bistability threshold of this hybrid cavity design is promising for various silicon photonic applications at telecom wavelengths requiring low-power optical nonlinearity. Our design provides a comparable threshold as observed in silicon photonic crystal cavities⁴⁶⁻⁴⁸ and ring cavities.⁴⁹⁻⁵¹

5. Conclusion

In summary, we have shown that low power threshold lasing and optical bistability can be achieved using a new Si-GaAs hybrid cavity design. In this approach, the cavity is patterned in the silicon waveguide while the GaAs slab features quantum dots that are optically active at telecom wavelengths. The hybrid device is facile to fabricate without careful alignment using simple pickup and placement by transfer printing method^{52,53} and can be practically implemented. Additionally, this hybrid device can operate at different frequencies by changing the cavity design parameters, with optimization enabling further

improved performance. Our work represents a critical step toward the efficient heterogeneous integration of silicon and III-V materials for future low-power silicon nanophononics.

Acknowledgement

Office of Naval Research (grant #N000142012551), ARL (grant #W911NF1920181), AFOSR-AOARD (grant #FA23862014072), and National Science Foundation (Grants #OMA1936314, #ECCS1933546, #PHY1839165).

References

1. Zhou, Zhiping, Bing Yin, and Jurgen Michel. "On-chip light sources for silicon photonics." *Light: Science & Applications* 4.11 (2015): e358-e358.
2. Tran, Minh A., Duanni Huang, and John E. Bowers. "Tutorial on narrow linewidth tunable semiconductor lasers using Si/III-V heterogeneous integration." *APL photonics* 4.11 (2019): 111101.
3. Ramirez, Joan Manel, et al. "III-V-on-silicon integration: from hybrid devices to heterogeneous photonic integrated circuits." *IEEE Journal of Selected Topics in Quantum Electronics* 26.2 (2019): 1-13.
4. Tran, Minh A., et al. "Ultra-low-loss silicon waveguides for heterogeneously integrated silicon/III-V photonics." *Applied Sciences* 8.7 (2018): 1139.
5. Xiao, Zhe, et al. "Ultra-compact low loss polarization insensitive silicon waveguide splitter." *Optics Express* 21.14 (2013): 16331-16336.
6. Zemtsov, Daniil S., et al. "Broadband silicon grating couplers with high efficiency and a robust design." *Optics Letters* 47.13 (2022): 3339-3342.
7. D. Taillaert, P. Bienstman, and R. Baets, "Compact efficient broadband grating coupler for silicon-on-insulator waveguides," *Opt. Lett.* 29, 2749 (2004).
8. Zhang, Jing, et al. "Silicon waveguide based TE mode converter." *Optics Express* 18.24 (2010): 25264-25270.
9. Koonen, A. M. J., et al. "Silicon photonic integrated mode multiplexer and demultiplexer." *IEEE Photonics Technology Letters* 24.21 (2012): 1961-1964.
10. Gong, Yiyang, et al. "Nanobeam photonic crystal cavity quantum dot laser." *Optics express* 18.9 (2010): 8781-8789.
11. Bimberg, Dieter, and Nikolai Ledentsov. "Quantum dots: lasers and amplifiers." *Journal of Physics: Condensed Matter* 15.24 (2003): R1063.
12. Hiraki, Tatsuro, et al. "Heterogeneously integrated iii-v/si mos capacitor mach-zehnder modulator." *Nature Photonics* 11.8 (2017): 482-485.
13. Buyukkaya, Mustafa Atabey, et al. "Low power optical bistability from quantum dots in a nanobeam photonic crystal cavity." *Applied Physics Letters* 121.8 (2022): 081104.
14. Komljenovic, Tin, et al. "Photonic integrated circuits using heterogeneous integration on silicon." *Proceedings of the IEEE* 106.12 (2018): 2246-2257.
15. Lee, Jungmin, et al. "Printed nanolaser on silicon." *ACS Photonics* 4.9 (2017): 2117-2123.
16. Halioua, Yacine, et al. "Hybrid III-V semiconductor/silicon nanolaser." *Optics express* 19.10 (2011): 9221-9231.
17. Bazin, Alexandre. III-V Semiconductor Nanocavities on Silicon-On-Insulator Waveguide: Laser Emission, Switching and Optical Memory. Diss. Université Paris-Diderot-Paris VII, 2013.

18. Crosnier, Guillaume, et al. "Hybrid indium phosphide-on-silicon nanolaser diode." *Nature Photonics* 11.5 (2017): 297-300.
19. Osada, Alto, et al. "Transfer-printed quantum-dot nanolasers on a silicon photonic circuit." *Applied Physics Express* 11.7 (2018): 072002.
20. Mitze, T., et al. "Hybrid integration of III/V lasers on a silicon-on-insulator (SOI) optical board." *IEEE International Conference on Group IV Photonics*, 2005. 2nd. IEEE, 2005.
21. Park, Hyundai, et al. "Hybrid silicon evanescent laser fabricated with a silicon waveguide and III-V offset quantum wells." *Optics Express* 13.23 (2005): 9460-9464.
22. Fang, Alexander W., et al. "A continuous-wave hybrid AlGaInAs-silicon evanescent laser." *IEEE Photonics Technology Letters* 18.10 (2006): 1143-1145.
23. H. Park, A. W. Fang, O. Cohen, R. Jones, M. J. Paniccia, and J. E. Bowers, "A hybrid Al- GaInAs-silicon evanescent amplifier," *IEEE Photon. Technol. Lett.* 19(4), 230–2232 (2007).
24. Liu, Liu, et al. "Carrier-injection-based electro-optic modulator on silicon-on-insulator with a heterogeneously integrated III-V microdisk cavity." *Optics letters* 33.21 (2008): 2518-2520.
25. Taflove, *Computational Electromagnetics: The Finite-Difference Time-Domain Method*. Boston: Artech House, (2005).
26. S.-H. Chang and A. Taflove, "Finite-difference time-domain model of lasing action in a four-level two-electron atomic system," *Opt. Express* 12(16), 3827 (2004).
27. Gong, Yiyang, et al. "Nanobeam photonic crystal cavity quantum dot laser." *Optics express* 18.9 (2010): 8781-8789.
28. Yanik, Mehmet Fatih, Shanhui Fan, and Marin Soljačić. "High-contrast all-optical bistable switching in photonic crystal microcavities." *Applied Physics Letters* 83.14 (2003): 2739-2741.
29. Pelton, M. Modified spontaneous emission in nanophotonic structures. *Nat. Photon.* 9, 427–435 (2015).
30. Bjork, Gunnar, and Yoshihisa Yamamoto. "Analysis of semiconductor microcavity lasers using rate equations." *IEEE Journal of Quantum Electronics* 27.11 (1991): 2386-2396
31. Yang, Zhili, et al. "A room temperature continuous-wave nanolaser using colloidal quantum wells." *Nature communications* 8.1 (2017): 1-8.
32. Wu, Sanfeng, et al. "Monolayer semiconductor nanocavity lasers with ultralow thresholds." *Nature* 520.7545 (2015): 69-72.
33. Mario, Landobasa Y., S. Darmawan, and Mee K. Chin. "Asymmetric Fano resonance and bistability for high extinction ratio, large modulation depth, and low power switching." *Optics express* 14.26 (2006): 12770-12781.
34. Tanabe, Takasumi, et al. "Fast bistable all-optical switch and memory on a silicon photonic crystal on-chip." *Optics letters* 30.19 (2005): 2575-2577.
35. Xu, Qianfan, and Michal Lipson. "All-optical logic based on silicon micro-ring resonators." *Optics express* 15.3 (2007): 924-929.
36. Fleming, R. M., et al. "Defect-driven gain bistability in neutron damaged, silicon bipolar transistors." *Applied physics letters* 90.17 (2007): 172105.
37. Sridharan, Deepak, and Edo Waks. "All-optical switch using quantum-dot saturable absorbers in a DBR microcavity." *IEEE Journal of Quantum Electronics* 47.1 (2010): 31-39.
38. Zhao, Yuqi, Hamidreza Chalabi, and Edo Waks. "Low power threshold, ultrathin optical limiter based on a nonlinear zone plate." *Optics Express* 29.21 (2021): 33144-33154.

39. D. Guimard, M. Nishioka, S. Tsukamoto, and Y. Arakawa, "High density InAs/GaAs quantum dots with enhanced photoluminescence intensity using antimony surfactant-mediated metal organic chemical vapor deposition," *Appl. Phys. Lett.* 89(18), 183124 (2006).
40. H. Fujita, K. Yamamoto, J. Ohta, Y. Eguchi, and K. Yamaguchi, "In-plane quantum-dot superlattices of InAs on GaAsSb/GaAs(001) for intermediate band solar-cells," *Conf. Rec. IEEE Photovolt. Spec. Conf.* 001, 002612–002614 (2011).
41. C. H. Lin, H. S. Lin, C. C. Huang, S. K. Su, S. D. Lin, K. W. Sun, C. P. Lee, Y. K. Liu, M. D. Yang, and J. L. Shen, "Temperature dependence of time-resolved photoluminescence spectroscopy in InAs/GaAs quantum ring," *Appl. Phys. Lett.* 94(18), 13–16 (2009).
42. P. Borri, W. Langbein, J. Mørk, J. M. Hvam, F. Heinrichsdorff, M. H. Mao, and D. Bimberg, "Dephasing in InAs/GaAs quantum dots," *Phys. Rev. B* 60(11), 7784–7787 (1999).
43. Bonifacio, R., and L. A. Lugiato. "Optical bistability and cooperative effects in resonance fluorescence." *Physical Review A* 18.3 (1978): 1129.
44. H.M. Gibbs, *Optical bistability: controlling light with light.* (Academic Press, Orlando, 1985).
45. Fryett, Taylor K., Christopher M. Dodson, and Arka Majumdar. "Cavity enhanced nonlinear optics for few photon optical bistability." *Optics express* 23.12 (2015): 16246-16255.
46. Laurent-Daniel Haret, Takasumi Tanabe, Eiichi Kuramochi, and Masaya Notomi, "Extremely low power optical bistability in silicon demonstrated using 1D photonic crystal nanocavity," *Opt. Express* 17, 21108-21117 (2009)
47. M. Notomi, A. Shinya, S. Mitsugi, G. Kira, E. Kuramochi, and T. Tanabe, "Optical bistable switching action of Si high-Q photoniccrystal nanocavities," *Opt. Exp.*, vol. 13, no. 7, pp. 2678–2687, Apr. 2005.
48. Takasumi Tanabe, Masaya Notomi, Satoshi Mitsugi, Akihiko Shinya, and Eiichi Kuramochi, "Fast bistable all-optical switch and memory on a silicon photonic crystal on-chip," *Opt. Lett.* 30, 2575-2577 (2005).
49. Y. Zhang et al., "Ultralow Power Nonlinear Response in an Si Photonic Crystal Nanocavity," in *IEEE Photonics Journal*, vol. 5, no. 4, pp. 6601409-6601409, Aug. 2013, Art no. 6601409, doi: 10.1109/JPHOT.2013.2273734.
50. Almeida, Vilson R., and Michal Lipson. "Optical bistability on a silicon chip." *Optics letters* 29.20 (2004): 2387-2389.
51. Peng Sun and Ronald M. Reano, "Low-power optical bistability in a free-standing silicon ring resonator," *Opt. Lett.* 35, 1124-1126 (2010).
52. Kim, Je-Hyung, et al. "Hybrid integration methods for on-chip quantum photonics." *Optica* 7.4 (2020): 291-308.
53. Yoon, Jongseung, et al. "Heterogeneously integrated optoelectronic devices enabled by micro-transfer printing." *Advanced Optical Materials* 3.10 (2015): 1313-1335.